Nanosheets

DOI: 10.1002/anie.201104299

One-Step Synthesis of Bismuth Telluride Nanosheets of a Few Quintuple Layers in Thickness**

*Yimin Zhao, Robert W. Hughes, Zixue Su, Wuzong Zhou, and Duncan H. Gregory**

Strictly two dimensional (2D) crystals were previously believed to be non-existent due to inherent thermodynamical instability.[1] Thin films of quasi 2D crystals had been limited until recently to epitaxial growth on single-crystal substrates with lattice matching achieved by routes such as molecular beam epitaxy (MBE).[2] Graphene, 2D monolayers of graphite, was first observed experimentally in 2004 to exist as single layer (or 2–3 layer) freestanding films.[3] It was explained that 2D crystals become intrinsically stable by gentle "crumpling" in the third dimension.[4] Some inorganic, quasi-2D compounds, such as dichalcogenides (WS_2 and MoS_2),[5] boron nitride (BN)[6,7] and some complex oxides[8] have been prepared by mechanical cleavage or chemical intercalation/exfoliation methods.

Bismuth telluride, Bi_2Te_3, as one of the best known thermoelectric materials, possesses the highest figure of merit and power factor at room temperature.[9,10] Calculations have shown that 2D Bi_2Te_3 layers in a quantum well structure have the potential to increase the figure of merit by a factor of 13 over the bulk telluride.[11] Very recently, mechanical exfoliation techniques similar to those used in the preparation of graphene were employed by Teweldebrhan et al. to prepare the first 2D Bi_2Te_3 crystals.[12] Experiments indicate that these 2D Bi_2Te_3 crystals possess a high electrical conductivity and low thermal conductivity[13] and Bi_2Te_3 2D thin films present a new class of topological insulators.[14,15] Also, very recently, rigid triangular and hexagonal Bi_2Q_3 (Q = Se,Te) nanoplates of 6 nm or less in thickness were deposited from the respective bulk chalcogenide powders.[16] Here, we report the facile, one-step synthesis and growth of 2D Bi_2Te_3 nanosheets using chemical vapor transport (CVT) methods in a sealed tube. The surface-assisted CVT (SACVT) technique used here[17] is a low-cost and uncomplicated synthesis method that can be used for producing a relatively high yield of nanomaterials. Performing the reaction in a closed container means that departures from the target stoichiometry of the products can be minimized. The folded edges of the nanometer scale sheets in the reactions described here provide a clear high-resolution transmission electron microscopy (HRTEM) signature for the exact thickness of the 2D Bi_2Te_3 crystals.

Figure 1 shows a (negative) SEM image of the products deposited on the as-received Si wafer after the reaction. From the SEM image we can see that most of the particles have a thin sheet-like morphology and many edges of the particles

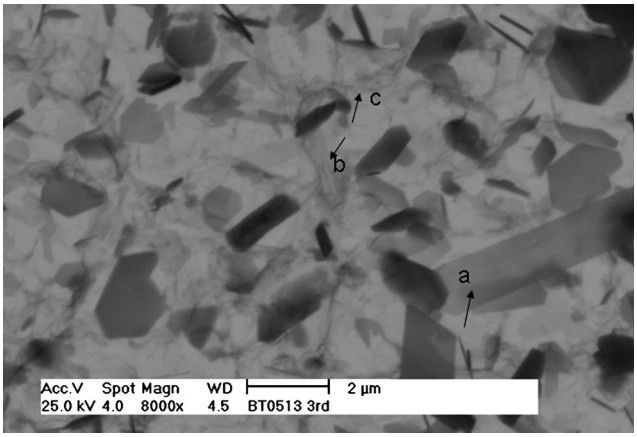

Figure 1. SEM image (negative) of the Bi_2Te_3 nanosheets on the Si substrate.

are organized at a 120° or 60° angle, indicating a possible hexagonal crystal structure. The thin sheets are typically approximately a few micrometers in width. In the arrowed areas in Figure 1, we can see two thin sheets stacking together (arrow **a**) and it is clear that the top sheet is transparent. There are also areas (arrows **b** and **c**) with a much weaker contrast that resemble very thin films that are strongly crumpled on the surface.

The powder X-ray diffraction (XRD) pattern of the product is shown in Figure 2. With the exception of the peak for the underlying Si substrate, all other peaks match well with rhombohedral Bi_2Te_3 (ICDD PDF card No. 01-089-2009, $a = 4.386$ Å, $c = 30.497$ Å) with no evidence of other phases. Rietveld refinement[18] finally converged to $R_{wp} = 0.0847$ and $R_p = 0.0569$ to yield a structure in rhombohedral space group $R\bar{3}m$ with lattice parameters of $a = 4.3856(1)$ Å, $c = 30.503(1)$ Å (see Supporting Information). The sample exhibited preferred orientation in the [001] direction.

The unit cell contains three formula units, as shown in Figure 3a and the structure is built up of quintuple layers (QL) that are stacked in a sequence of Te(1)-Bi-Te(2)-Bi-

[*] Dr. Y. Zhao, Dr. R. W. Hughes, Prof. D. H. Gregory
WestCHEM, School of Chemistry, University of Glasgow
Glasgow G12 8QQ (UK)
E-mail: duncan.gregory@glasgow.ac.uk
Dr. Z. Su, Prof. W. Zhou
EaStCHEM, School of Chemistry, University of St Andrews
St Andrews, Fife KY16 9ST (UK)

[**] D.H.G. thanks the EPSRC and Dstl for funding this work under grant EP/H020543/1. The authors thank EPSRC's support for the free access to the TEM/SEM facility at the University of St. Andrews and acknowledge use of the EPSRC's Chemical Database Service (ICSD).

Supporting information for this article is available on the WWW under http://dx.doi.org/10.1002/anie.201104299.

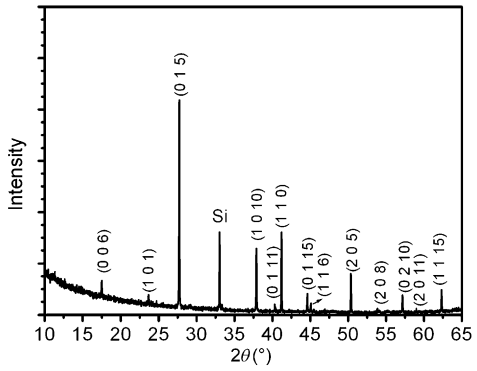

Figure 2. XRD pattern from Bi_2Te_3 nanosheets.

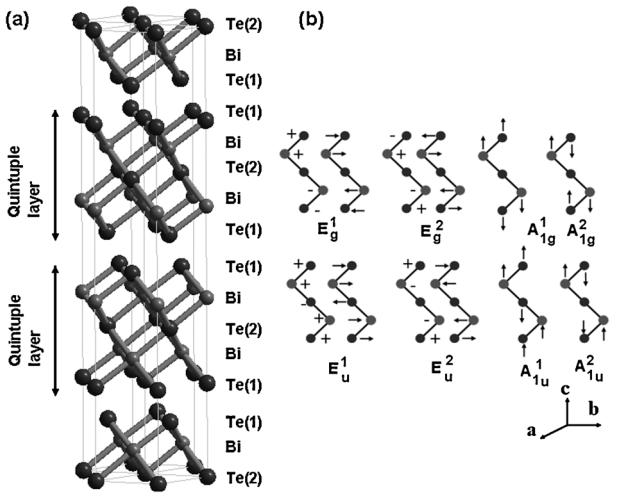

Figure 3. a) Layered crystal structure of Bi_2Te_3. Bi atoms are coordinated to six Te atoms in octahedral geometry. b) Schematic of the lattice vibrations (12 optical modes) in a Te(1)-Bi-Te(2)-Bi-Te(1) quintuple layer (QL). The subscripts "1" and "2" to the labels E_g, A_{1g}, E_u, and A_{1u} denote the low and high frequency modes, respectively; "E" and "A" modes refer to the in-plane (*ab* plane) and out-of-plane (*c* axis) vibrations. "+" and "−" designate the atomic displacement towards and from the observer, respectively.

Te(1). Here, Te has two different coordination environments in the crystal structure. Te(1) is bonded to three Bi atoms in the same QL and interacts with three Te(1) atoms in the adjacent QL by van der Waals forces. Te(2) atoms are coordinated almost octahedrally by six Bi atoms. Bi atoms are bonded to three Te(1) atoms and three Te(2) atoms. The QLs are thus coupled by weak van der Waals interactions along the *c* direction. These anisotropic crystal characteristics make it a good candidate for 2D crystal growth. Similar to other 2D crystals prepared by chemical vapor techniques, such as graphene, boron nitride or bismuth selenide, thin Bi_2Te_3 nanosheets prepared by the CVT technique (Figure 1) may exhibit a hexagonal or triangular shape, which would be expected to arise from the fact that the 2D crystals grow laterally in the basal plane of the hexagonal structure which has six-fold symmetry.

Figure 4a shows the low magnification TEM image of a typical Bi_2Te_3 nanosheet. The ripple-like contrasts are caused

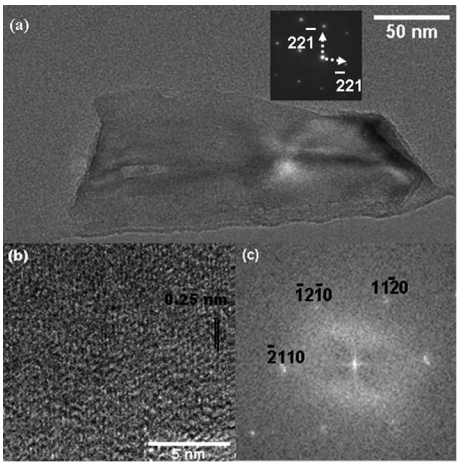

Figure 4. a) Low-magnification TEM image of a Bi_2Te_3 nanosheet. The inset is the corresponding SAED pattern viewed down the $[\bar{1}01\bar{2}]$ direction; b) HRTEM of the 2D nanosheet and c) the corresponding FFTED pattern from the sheet shown in (b) in the [0001] projection.

by the strain from the bending of the super-thin structure.[19] The EDX spectrum from the nanosheet (see Supporting Information) further confirms that the nanosheets are composed only of Bi and Te. The selected area electron diffraction (SAED) pattern (inset of Figure 4a) demonstrates the single-crystalline nature of the super-thin Bi_2Te_3 nanosheet. The SAED pattern can be identified to the $[\bar{1}01\bar{2}]$ projection of the hexagonal Bi_2Te_3 reciprocal lattice. Figure 4b displays the higher resolution TEM (HRTEM) image of the Bi_2Te_3 nanosheet and the corresponding fast Fourier transformation electron diffraction (FFTED) pattern. The FFTED pattern has six-fold symmetry and can be identified as the [0001] projection of the hexagonal Bi_2Te_3 reciprocal lattice, which indicates that the top and bottom faces of the nanosheet are {0001} planes. The measured spacing between the lattice fringes in the HRTEM images in Figure 4b is ca. 0.24 nm, which is slightly larger than the *d* spacing (0.219 nm) of the $\{11\bar{2}0\}$ planes of the bulk specimen.

Figure 5a shows a low magnification TEM image of strongly crumpled Bi_2Te_3 nanosheets. HRTEM images of the curved edges or folded areas of graphene have been used to determine the exact number of the graphene layers.[4] In the present work, the SAED patterns of the strongly crumpled nanosheets were recorded to confirm the single-crystalline property of the nanosheets. Some higher magnification images of the edges of the Bi_2Te_3 nanosheet are shown in Figure 5b,c. The curved edge of the Bi_2Te_3 nanosheet in Figure 5b shows lattice fringes of two dark lines with a thickness about 3 nm. This spacing is very close to the unit cell dimension along the *c* axis of the hexagonal Bi_2Te_3, further confirming that the Bi_2Te_3 nanosheet grows vertical to the *c* axis of hexagonal Bi_2Te_3. Another typical higher magnification TEM image of the folded areas of the crumpled nanosheet shown in Figure 5c shows fringes comprised of three dark lines with the total thickness of the fringes in a range of 6.02–6.44 nm. Consequently, the thickness of these nanosheets matches two unit cells along the *c* axis. Unlike some perfectly flat thin plates of inorganic compounds, where

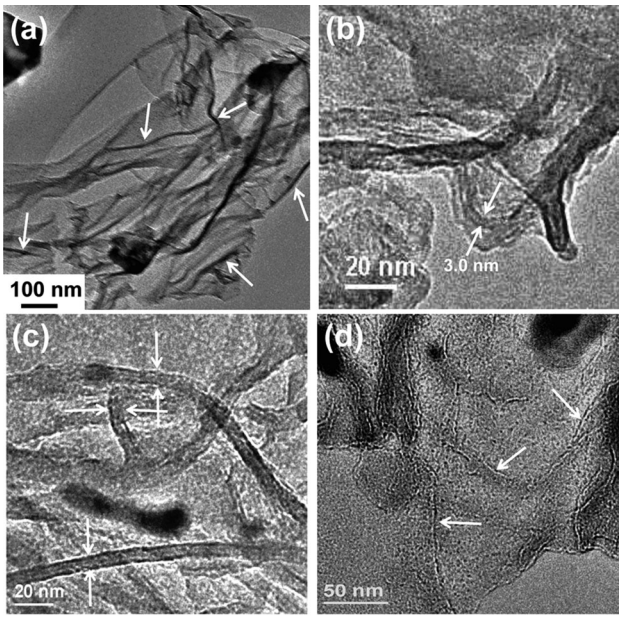

Figure 5. a) Low-magnification TEM image of strongly crumpled Bi_2Te_3 nanosheets. The arrows indicate the edges of the nanosheets with a thickness of ca. 6 nm. b) Higher-magnification TEM image of a nanosheet showing an edge (two dark lines) ca. 3 nm in thickness as indicated by the arrows. c) Folded areas of the nanosheets exhibiting fringes (three dark lines indicated by the arrows) with a sheet thickness of ca. 6 nm. d) TEM image of some very thin nanosheets, probably less than three QLs in thickness.

atomic resolution HRTEM profile images can be recorded to show individual atomic layers,[20] atomic layers and even a single QL (about 1 nm in thickness), cannot be imaged from these heavily crumpled nanosheets. When the nanosheets are thick, the edges are not bent and profile images as shown in Figure 4a could not be recorded. Figure 5d shows some examples of overlapping nanosheets and in these cases the edges of the individual nanosheets can be seen. However, the exact thicknesses of the nanosheets cannot be revealed.

The 2D anisotropic crystal growth is believed to be steered by the intrinsic anisotropic bonding characteristics of the hexagonal Bi_2Te_3 structure (see Figure 3), similar to the growth of Bi_2Te_3 and Bi_2Se_3 nanoplates by catalyst-free chemical vapor deposition (CVD) techniques.[16] After nucleation the atoms preferentially close-pack hexagonally along the basal plane rather than along the *c* axis in order to minimize the surface energy when growing, leading to anisotropic growth. The Bi_2Te_3 nanosheets may consist of an integer or non-integer number of QLs. From our observations, the substrate temperature, which has the capacity to mediate suitable nucleation and growth rates, is the most important factor for 2D anisotropic growth. This substrate temperature requires fine control: at temperatures higher than 380 °C bulk Bi_2Te_3 was formed and at temperatures lower than 340 °C irregular particles were deposited on the substrate (see Supporting Information).

The Raman spectra of Bi_2Te_3 nanosheets and bulk Bi_2Te_3 as a reference are shown in Figure 6. Bulk Bi_2Te_3 has 12 optical modes that can be classified into 2 A_{1g}, 2 E_g, 2 E_u, and 2 A_{1u}. The atomic displacement schematics are shown in Figure 3b. Shahil et al. first reported the Raman pattern of 2D crystals a few QL in thickness in samples prepared by mechanical exfoliation techniques.[21] The assignment of the Raman bands is summarized in Table 1.[21] The four Raman active modes E_g^1, A_{1g}^1, E_g^2, and A_{1g}^2 are observed in bulk Bi_2Te_3 at 40.2 cm^{-1}, 60.2 cm^{-1}, 100.8 cm^{-1}, and 133.2 cm^{-1} respectively, which are consistent with the literature.[21,22]

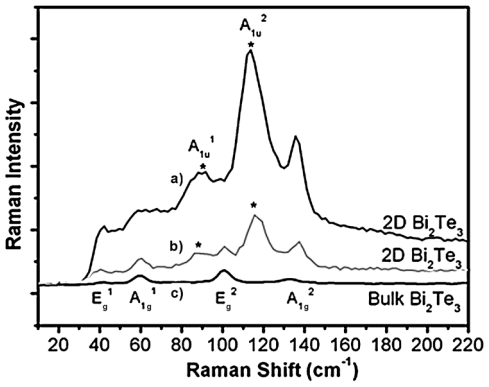

Figure 6. Raman spectra of Bi_2Te_3 nanosheets (from two different areas of the same sample; spectra a and b) and bulk Bi_2Te_3 (spectrum c).

Table 1: Raman bands in bulk Bi_2Te_3 and 2D nanosheets.

	E_g^1	A_{1g}^1	A_{1u}^1	E_g^2	A_{1u}^2	A_{1g}^2	Ref.
bulk	40.2	60.2	–	100.8	–	133.2	this work
2D(b)	40.1	59.1	87.8	100.8	115.2	137.2	this work
2D(a)	38.9	58.7	86.4	98.8	113.9	135.6	this work
bulk	34.4	62.1	–	101.7	–	134.0	[21]
40 nm	38.9	61.3	–	107.3	116.2	133.0	[21]
4 nm	38.9	60.9	–	101.4	116.7	132.9	[21]

The Raman spectra were reproducible at different spots on the as-prepared Bi_2Te_3 nanosheets on the Si substrate, and typically two kinds of spectra with higher and lower signal intensity were obtained (Figure 6; spectrum a and b, respectively). As shown from the SEM and TEM images, the Bi_2Te_3 nanosheets deposited on the Si substrate are not uniform in thickness. The nanosheets with hexagonal morphology are observed to be thicker than the crumpled, large-area nanosheets (which are as thin as 1–2 QL) as indicated from the contrast in the SEM image (Figure 1). The stronger Raman signal may be due to the very thin crumpled nanosheets, while the weaker Raman signal may be due to the hexagonal nanosheets as the peak intensity typically becomes stronger with a decrease in thickness of Bi_2Te_3 exfoliated flakes.[23]

In addition to the four Raman modes shown in bulk Bi_2Te_3, two more bands at ca. 88 cm^{-1} and 114 cm^{-1}, respectively, were observed in this work for the Bi_2Te_3 nanosheets. In Ref. [21], a band at ca. 117 cm^{-1} for 4 nm thick Bi_2Te_3 films was assigned to an A_{1u} mode because of the loss of extended dimensionality along the *c*-axis. The infrared-active A_{1u}^1 and A_{1u}^2 modes at 94 cm^{-1} and 120 cm^{-1} have been

observed from FTIR studies in bulk crystalline Bi_2Te_3 (but are absent in the experimental Raman spectrum as expected).[22] Here, the additional bands at 88 cm^{-1} and 114 cm^{-1} in our CVT materials can be assigned to the $A_{1u}{}^1$ and $A_{1u}{}^2$ modes, respectively. Based on the selection rules,[23] the four optical modes denoted by u subscripts are Raman-inactive (IR-active) because they are odd parity modes (the displacement at a lattice site does not change sign under a inversion operation).[24] Due to the high surface to volume ratio of the free-standing 2D nanosheets, surface effects play an important role in determining the chemical and physical properties.[25] Molecular dynamics (MD) studies of free-standing Bi_2Te_3 nanofilms with a thickness ranging from 3 to 15 nm have predicted that the *c* lattice constant expands to 3.14 nm while there are no obvious changes to in-plane dimensions.[26] Whereas this expansion is not manifested in an average, long-range structure analysis such as that we have performed by Rietveld refinement against XRD data, we do see some evidence of such expansions in individual sheets on a microscopic level from fringe spacing measurements in the HRTEM. Based on the MD simulation results[25] the surface of the nanofilm undergoes tensile stress whereas the bulk (internal) structure undergoes compressive stress. As discussed before, the Bi_2Te_3 nanosheets prepared by the CVT technique may have an uncompleted QL at the surface. Atoms on and near the surface will lose some neighbour atoms and electron density, possess higher energies and are more likely to move out of the plane[26] and thus break the symmetry along the *c* axis and make the $A_{1u}{}^1$ and $A_{1u}{}^2$ modes Raman active. The $A^1{}_g{}^1$ band shifts to lower wavenumber with nanosheet thickness as had been previously observed.[21]

It can be seen from Figure 6 that vibration modes with a lattice displacement along the *c* axis become stronger than those with a displacement in the *ab* plane of the nanosheets by comparing the intensity ratio, $I(A^1{}_g{}^2/E_g{}^2)$. Similar phenomena were also observed from 2D crystals of Bi_2Te_3 that were four QLs thick and prepared by mechanical exfoliation techniques.[21]

In summary, two-dimensional Bi_2Te_3 nanosheets have been synthesized on an as-received Si wafer substrate by surface-assisted CVT technique; a methodology that could also find application in the synthesis of other chalcogenide nanostructures. HRTEM characterization of the curved edges and folded areas of the crumpled Bi_2Te_3 nanosheets indicated that the Bi_2Te_3 nanosheets grow in the basal plane of the hexagonal Bi_2Te_3 structure and are typically a few nm in thickness, equivalent to 1–6 quintuple layers. Raman studies found that modes ($A_{1u}{}^1$ and $A_{1u}{}^2$) that are inactive in bulk Bi_2Te_3 and involve atom displacement along the *c* axis become Raman-active in the Bi_2Te_3 nanosheets due to crystal symmetry breaking perpendicular to the *ab* plane. Further characterizations of the properties of the 2D Bi_2Te_3 nanosheets, such as the electronic and thermal properties are still under investigation to explore their applications as one of the most important thermoelectric materials and topological insulators.

Experimental Section

Bi_2Te_3 nanosheets were synthesized by CVT methods in a sealed system. In a typical reaction, elemental powders of Bi (0.2 mmol; BDH, ingot, $\geq$ 99 %) and Te (0.3 mmol; Fluka, purum) were ground together and placed at one end of a 12 mm diameter fused silica tube. A Si substrate was placed 14 cm away from the source materials. The Si substrate was held in a vertical position (i.e. oriented perpendicular to the long axis of the tube) by a quartz holder placed inside the fused silica tube, as shown in Figure S5 (see Supporting Information). The silica tube was sealed under a pressure of $6–7 \times 10^{-2}$ Torr and placed horizontally in a tube furnace heated to 700 °C for 24 h such that the source materials were placed at the hot centre of the tube furnace and the substrate was placed at a colder zone (i.e. 14 cm away from the hot furnace centre at 350–360 °C, as measured by a thermocouple). After the reaction the fused silica tube was air quenched to room temperature and opened.

The as-grown nanostructures on the Si substrate were directly characterized by SEM (Philips XL30 SEM, operated at 20 kV in high-vacuum mode with 5 mm working distance). Phase purity and crystal structure were analyzed by powder X-ray diffraction (XRD) (Panalytical X'Pert PRO MPD diffractometer; $\theta-2\theta$; $CuK_{\alpha 1}$ radiation, flat plate configuration). Data were collected as step scans with step intervals of 0.017° over a range of $5 \leq 2\theta/° \leq 70$ with a time per step of 2 s. Rietveld refinement against the XRD data was performed using the General Structure Analysis System (GSAS) through the Windows-based EXPGUI interface.[27,28] TEM characterization was performed using a JEOL TEM 2011 equipped with an EDX system, operating at 200 kV. To prepare the TEM sample, the Bi_2Te_3 nanosheets were physically removed from the Si substrate, dispersed in acetone and sonicated for 2 min to obtain a uniform suspension. 1–2 drops of the suspension were dropped onto a 3 mm diameter holey carbon-coated Cu TEM grid for the TEM analysis. Raman spectra were collected for bulk samples and nanosheets of Bi_2Te_3 using a Horiba–Jobin–Yvon LabRam HR confocal microscope, equipped with a Quantum Ventus 532 laser at 150 mW, excited with 532 nm light. All spectra were collected through a 50× objective lens in backscattering mode with a 600 g mm^{-1} grating and a Synapse CCD detector. To minimize the burning effect, all spectra were collected by using ten times reduced incident laser power together with a 50 μm aperture.

Received: June 21, 2011
Revised: August 1, 2011
Published online: September 14, 2011

Keywords: bismuth · chalcogenides · chemical vapor transport · nanostructures · tellurium

[1] A. K. Geim, K. S. Novoselov, *Nat. Phys.* **2007**, *6*, 183 – 191.
[2] W. P. McCray, *Nat. Nanotechnol.* **2007**, *2*, 259 – 261.
[3] K. S. Novoselov, A. K. Geim, S. V. Morozov, D. Jiang, Y. Zhang, S. V. Dubonos, I. V. Grigorieva, A. A. Firsov, *Science* **2004**, *306*, 666 – 669.
[4] J. C. Meyer, A. K. Geim, M. I. Katsnelson, K. S. Novoselov, T. J. Booth, S. Roth, *Nature* **2007**, *446*, 60 – 63.
[5] H. S. S. R. Matte, A. Gomathi, A. K. Manna, D. J. Late, R. Datra, S. K. Pati, C. N. R. Rao, *Angew. Chem.* **2010**, *122*, 4153 – 4156; *Angew. Chem. Int. Ed.* **2010**, *49*, 4059 – 4062.
[6] D. Pacilé, J. C. Meyer, C. O. Girit, A. Zettl, *Appl. Phys. Lett.* **2008**, *92*, 133107.
[7] J. Kotakoski, C. H. Jin, O. Lehtinen, K. Suenaga, A. V. Krasheninnikov, *Phys. Rev. B* **2010**, *82*, 113404.
[8] K. S. Novoselov, D. Jiang, F. Schedin, T. J. Booth, V. V. Khotkevich, S. V. Morozov, A. K. Geim, *Proc. Natl. Acad. Sci. USA* **2005**, *102*, 10451 – 10453.

[9] C. B. Satterthwaite, R. W. Ure, *Phys. Rev.* **1957**, *108*, 1164 – 1170.
[10] D. A. Wright, *Nature* **1958**, *181*, 834 – 834.
[11] L. D. Hicks, M. S. Dresselhaus, *Phys. Rev. B* **1993**, *47*, 12727 – 12731.
[12] D. Teweldebrhan, V. Goyal, A. A. Balandin, *Nano Lett.* **2010**, *10*, 1209 – 1218.
[13] D. Teweldebrhan, V. Goyal, M. Rahman, A. A. Balandin, *Appl. Phys. Lett.* **2010**, *96*, 053107.
[14] V. Goyal, D. Teweldebrhan, A. A. Balandin, *Appl. Phys. Lett.* **2010**, *97*, 133117.
[15] M. Z. Hossain, S. L. Rumyantsev, K. M. F. Shahil, D. Teweldebrhan, M. Shur, A. A. Balandin, *ACS Nano* **2011**, *5*, 2657 – 2663.
[16] D. S. Kong, W. H. Dang, J. J. Cha, H. Li, S. Meister, H. Peng, Z. F. Liu, Y. Cui, *Nano Lett.* **2010**, *10*, 2245 – 2250.
[17] C. W. Dunnill, H. K. Edwards, P. D. Brown, D. H. Gregory, *Angew. Chem.* **2006**, *118*, 7218 – 7221; *Angew. Chem. Int. Ed.* **2006**, *45*, 7060 – 7063.
[18] H. M. Rietveld, *J. Appl. Crystallogr.* **1969**, *2*, 65 – 71.
[19] X. Y. Kong, Y. Ding, R. Yang, Z. L. Wang, *Science* **2004**, *303*, 1348 – 1351.
[20] W. Z. Zhou, A. I. Kirkland, A. Porch, K. D. Mackay, A. R. Armstrong, M. R. Harrison, D. A. Jefferson, P. P. Edwards, W. Y. Liang, *Angew. Chem.* **1989**, *101*, 830 – 833; *Angew. Chem. Int. Ed. Engl.* **1989**, *28*, 810 – 813.
[21] K. M. F. Shahil, M. Z. Hossain, D. Teweldebrhan, A. A. Balandin, *Appl. Phys. Lett.* **2010**, *96*, 153103.
[22] W. Richter, H. Kouhler, C. R. Becker, *Phys. Status Solidi B* **1977**, *84*, 619 – 628.
[23] J. M. Friedman, R. M. Hochstrasser, *J. Am. Chem. Soc.* **1976**, *98*, 4043 – 4048.
[24] P. Y. Yu, M. Cardona, *Fundamentals of Semiconductors: Physics and Materials Properties*, 3rd ed. Springer, Heidelberg, **2005**.
[25] S. Urazhdin, D. Bilc, S. D. Mahanti, S. H. Tessmer, *Phys. Rev. B* **2004**, *69*, 085313.
[26] Y. Tong, F. Yi, L. Liu, P. Zhai, Q. Zhang, *Physica B* **2010**, *405*, 3190 – 3194.
[27] A. C. Larson, R. B. von Dreele, *The General Structure Analysis System*, **2000**, Los Alamos National Laboratories, Los Alamos.
[28] B. H. Toby, *J. Appl. Crystallogr.* **2001**, *34*, 210 – 213.

